Nano Research
2022, 15(9): 8465–8469

ISSN 1998-0124 CN 11-5974/O4
https://doi.org/10.1007/s12274-022-4410-7

Research Article

Molecular heterostructure by fusing graphene nanoribbons of different lengths through a pentagon ring junction

Qiang Sun[1,2] (✉), Hao Jiang[1], Yuyi Yan[1], Roman Fasel[2,3], and Pascal Ruffieux[2] (✉)

[1] *Materials Genome Institute, Shanghai University, Shanghai 200444, China*
[2] *Empa, Swiss Federal Laboratories for Materials Science and Technology, Dübendorf 8600, Switzerland*
[3] *Department of Chemistry, Biochemistry and Pharmaceutical Sciences, University of Bern, Bern 3012, Switzerland*

Received: 21 February 2022 / **Revised:** 3 April 2022 / **Accepted:** 8 April 2022

ABSTRACT

Graphene nanoribbons (GNRs) have attracted great research interest because of their widely tunable and unique electronic properties. The required atomic precision of GNRs can be realized via on-surface synthesis method. In this work, through a surface assisted reaction we have longitudinally fused the pyrene-based graphene nanoribbons (pGNR) of different lengths by a pentagon ring junction, and built a molecular junction structure on Au (111). The electronic properties of the structure are studied by scanning tunneling spectroscopy (STS) combined with tight binding (TB) calculations. The pentagon ring junction shows a weak electronic coupling effect on graphene nanoribbons, which makes the electronic properties of the two different graphene nanoribbons connected by a pentagon ring junction analogous to type I semiconductor heterojunctions.

KEYWORDS

graphene nanoribbons (GNRs), scanning tunneling spectroscopy (STS), non-contact atomic force microscopy (nc-AFM), tight-binding (TB) calculations, junction structure

1 Introduction

Graphene nanoribbons (GNRs) are highly promising nanomaterials for future electronic applications due to their tunable electronic properties that can be precisely determined by their widths and edge structures [1, 2]. Therefore, the key is to control the structure of graphene nanoribbons at the atomic level [3]. Different methods have been developed to manufacture graphene nanoribbons [4]. Among others, the bottom-up method, i.e., on-surface synthesis, stands as one of the most prominent ways [5, 6]. By employing ultrahigh vacuum (UHV) conditions together with the atomically clean and flat surfaces, on-surface synthesis provides significant advantages of achieving atomically precise nanostructures, while it also offers an ideal playground for the detailed characterization of the formed nanostructures. Recent studies reported the successful synthesis and characterization of armchair GNRs with different widths [7–11], chevron-type GNRs [12], zigzag GNRs [13], mixed edge structures [14, 15] as well as heteroatom-doped structures [16–18], to mention a few.

Due to lateral quantum confinement in GNRs, the two-dimensional electronic bands of the parent material graphene are reduced to a set of width-dependent one-dimensional (1D) bands with characteristic energy gaps [19]. This sensitive structure-properties relationship on one hand opens significant opportunities to achieve a wide range of electronic properties [20, 21], but on the other hand also requires atomic precision in GNR synthesis.

A further reduction of the allowed electronic states occurs for finite length GNR where the 1D bands of periodic infinite GNRs are reduced to a length-dependent number of discrete energy levels (schematically indicated in Fig. 1(a)). The 1D quantum well picture can be used to describe the system with the GNR ends behaving as walls of the potential well confining the electronic states. The energy levels of the finite system can therefore be approximately identified from the GNR bands by taking the energy levels at corresponding wave vectors $k(N) = \pm N\pi/L$, where N is the order of the confined frontier states and L represents the effective ribbon length [22, 23]. Consequently, the resulting highest occupied molecular orbital (HOMO)–lowest unoccupied molecular orbital (LUMO) gap of the finite GNRs is inversely proportional to the GNR length. In this work, we have studied a GNR junction structure that is formed by longitudinally connecting two GNR segments of different lengths with an atomically defined junction. We have applied high-resolution scanning probe microscopy imaging to identify the atomic structure of the connection between the GNR segments, which revealed a pentagon ring connecting the termini of two GNRs. Their electronic properties were investigated by scanning tunnelling spectroscopy (STS) in order to characterize the role of characteristic junctions and to compare it to finite pyrene-based graphene nanoribbons (pGNRs).

2 Results and discussion

Recently, we have reported synthesis of a low bandgap GNR (pGNR) which consists of covalently linked pyrene units achieved through activation of 1,6-dibromopyrene on the Au (111) surface under ultrahigh vacuum conditions [15]. The on-surface synthesis of pGNRs consists of two surface-assisted steps: (i) dehalogenative

Address correspondence to Qiang Sun, qiangsun@shu.edu.cn; Pascal Ruffieux, pascal.ruffieux@empa.ch

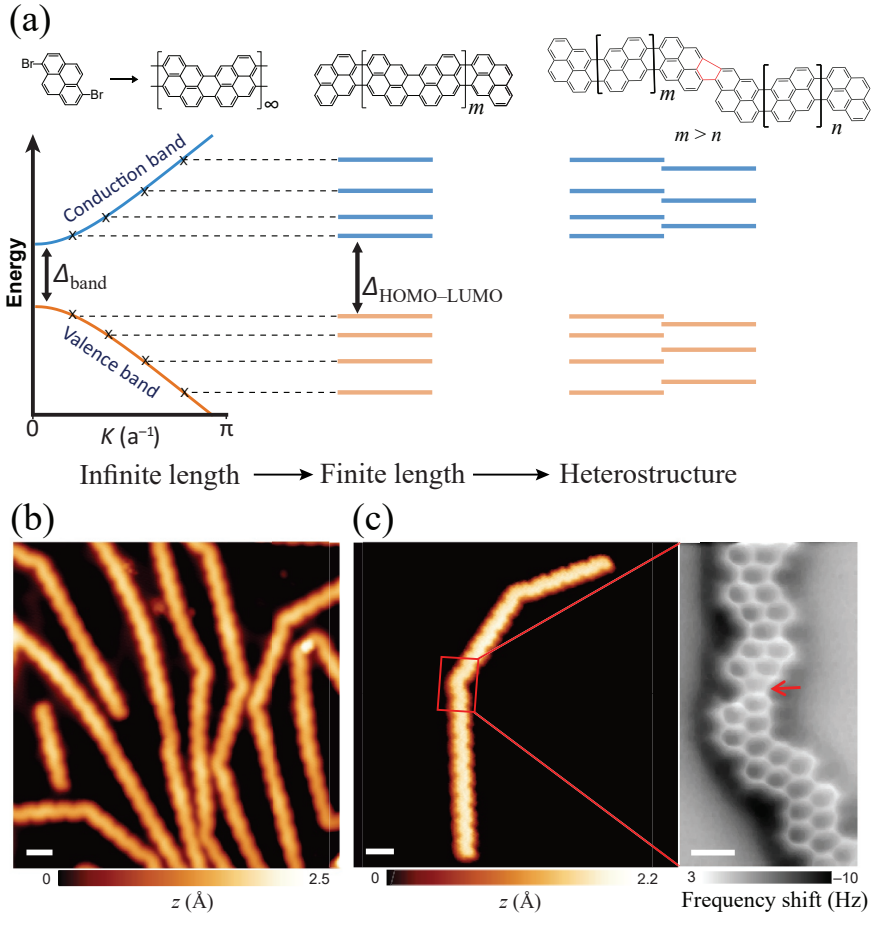

Figure 1 (a) Schematic representations of the synthesis of pGNRs with infinite length, finite length, and two pGNR segments fused by a 5-membered ring junction. In the bottom: the illustrative band structure and energy levels for the corresponding structures. The occupied band and energy levels are indicated in orange and the unoccupied ones in blue. The molecular energy levels of the finite-length pGNR can be approximated by the 1D quantum well model. (b) STM image of the sample obtained after annealing at 300 °C (V_s = 0.5 V and I_t = 50 pA). (c) STM image of a pGNR heterostructure composed of three pGNR segments (V_s = –0.2 V and I_t = 70 pA) and the nc-AFM image highlighting the kink, which is indicated by the red rectangle in the STM image (V_s = –5 mV and oscillation amplitude ≈ 80 pm, the red narrow indicates the 5-membered ring junction).

homocoupling yielding an intermediate polymer when annealing the substrate to 180 °C and (ii) cyclodehydrogenation-based formation of the fully conjugated ribbons at around 300 °C. In addition to the straight pGNRs terminated by pyrene subunits, kink structures are frequently observed as shown in a typical scanning tunnelling microscopy (STM) image in Fig. 1(b). Non-contact atomic force microscopy (nc-AFM) imaging with a CO functionalized tip has been applied to identify the atomic connectivity of the kinks [24], where we unequivocally recognize the fusion of two pGNR segments via a junction consisting of a 5-membered ring (indicated by the red arrow in Fig. 1(c)). The formation of the 5-membered ring junctions can be rationalized by the pyrene unit rotation that is involved in the cyclodehydrogenation step and appears to be unavoidable if the cyclodehydrogenation reaction starts in more than one position on the intermediate polymer [15]. If the last rotation step required for full planarization of the pGNR is not located at the pGNR terminus this would involve final rotation of a full pGNR segment with an exceedingly large energy barrier. An energetically more favorable reaction can be the formation of 5-membered ring junctions, as illustrated in Fig. S1 in the Electronic Supplementary Material (ESM). We note that similar 5-membered kinks were also observed in the growth of other GNRs of similar widths on surfaces [25, 26].

The formation of 5-membered ring junction as topological defects in graphene nanostructures can impact their electronic and magnetic properties [27, 28]. To determine the electronic properties of the pGNR heterostructure and the effect of 5-membered ring junctions, we have used STS to probe their local density of states. pGNR segments of different lengths embedded between two 5-membered ring junctions are analyzed. The STS results of these structures are compared with the STS results of the finite-length pGNR with open ends [15]. The determined energy positions of their frontier orbitals as a function of the number of the constituting pyrene unit are plotted in Fig. 2, where the HOMO–LUMO gap converges to 220 mV for ribbons with more than 25 monomer units. For a direct comparison, the HOMO/LUMO energy levels of the finite-length pGNRs were also plotted together with those of the fused pGNRs in Fig. 2. We clearly see that the energy levels of finite-length pGNRs follow very well with those of the fused pGNRs, and both of the structures converge to a HOMO–LUMO gap of 220 mV. Note that due to the energy level alignments caused by the different work functions of Au (111) and graphene structures, pGNR segments with more than 15 pyrene units are positively charged on the surface as manifested by the HOMO levels beyond the Fermi level [15, 29]. In addition, we did not observe any low bias features in the STS measurements of the fused pGNR, which indicates that the 5-membered ring junctions, although locally breaking the sublattice symmetry, do not induce spin polarization. These results indicate that the 5-membered ring junction behaves as a high-potential barrier that scatters electrons of the fused pGNR segments, in a way analogy to the open ends of finite-length pGNR [15].

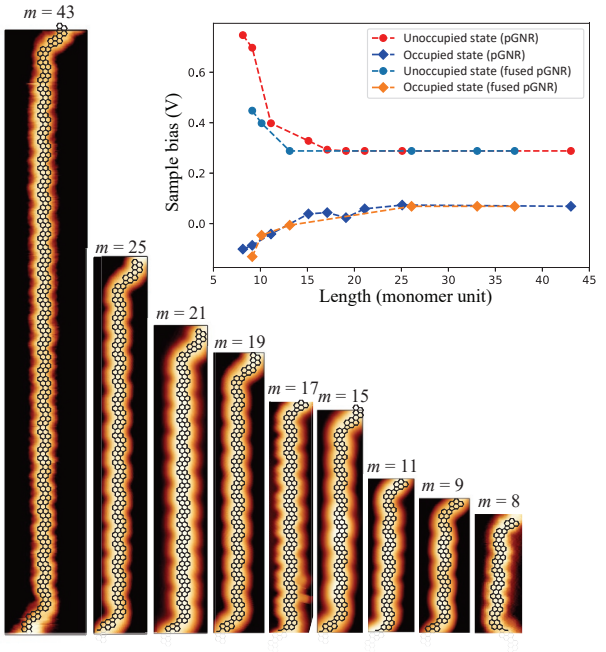

Figure 2 STM images of pGNR segments with different lengths (m represents the number of pyrene monomer units) and the inset: plot of the HOMO and LUMO energy levels of finite-length pGNR and fused pGNR.

We could further determine the band dispersions of the pGNR by plotting the frontier orbital energy positions of the fused pGNRs as a function of their corresponding wave vectors $k(N) = \pm N\pi/L$ (Fig. 3). As a result, the effective masses m^* and band onsets can be extracted through a parabolic fit $E(k) = E_{k=0} + \frac{(\hbar k)^2}{2m^*}$, where $\hbar$ is the reduced Planck's constant. The results are displayed in Fig. 3, from which we can derive a band gap E_g = 0.12 eV of pGNR on Au (111) and the effective mass m^* = 0.03 m_e for the valence band and m^* = –0.07 m_e for the conduction band, where m_e is the electron rest mass. It is worth to note that the energy band gap obtained by the parabolic fitting is about half of the directly measured HOMO–LUMO gap (about 230 meV, see Fig. 2). This discrepancy can be attributed to the Fermi level pinning of GNRs on Au(111) [30], which makes the energy positions of HOMO and LUMO converge pinned at low biases when the lengths of pGNR are beyond 25 monomer units and also results in the asymmetry of the conduction band (CB) and valence band (VB).

Further details on the junction properties become accessible when investigating fused pGNR segments of different lengths and hence different allowed energy levels. In particular, the different energy levels of the constituting pGNRs with different lengths raise an interesting question how the energy levels will align in the fused junction structures. Experimentally, we performed STS spectra on a 11/17 units fused pGNR junction structure observed on the Au(111) surface. STM image of the junction structure and the point spectra acquired on the corresponding pGNR segments are displayed in Fig. 4(a). The HOMO of the pGNR segments is reflected by prominent peaks in the spectra from which the energy positions are acquired, while the LUMO appears as bumps and the energy positions are determined by the edges of the maximum. Thus, the HOMO of 11 units pGNR is determined at –30 mV and its LUMO at 400 mV, while the HOMO of 17 units pGNR is at 40 mV and its LUMO at 300 mV (error for the positions of LUMO is in the range of a few mV). A STS line scan of the heterostructure (scan path indicated by green arrows in Fig. 4(b)) gives us further information on its spatially resolved orbital positions and how the energy positions shift at the junction site.

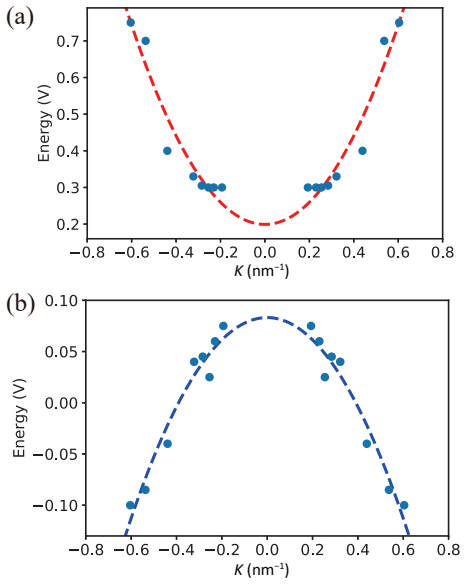

Figure 3 The band dispersions of the (a) CB and (b) VB of pGNR by fitting the orbital energy levels (blue dots) with parabola (dashed curves).

The color-coded map of the STS spectra acquired along the 11/17 fused heterostructure is shown in Fig. 4, where the frontier orbital levels are highlighted by dark dashed lines. We can clearly see an abrupt HOMO–LUMO gap shift occurring at the position close to the kink site as indicated by a red arrow in Fig. 4(b), and the HOMO–LUMO gap values change from 430 (pGNR with 11 units) to 260 mV (pGNR with 17 units). This energy level shift is reminiscent of the band shift in type I heterojunction, but in the form of discrete molecular level shift. Therefore, this molecular heterostructures and the molecular level shift could be useful for the realization of connected GNR-based quantum dots with applications in molecular electronics and optoelectronics. Note that we did not observe any odd-even effect for GNR heterostructures of different number of subunits.

Finally, tight binding (TB) calculations are carried out to give further insights on our experimental findings. We constructed two finite-length pGNRs, one with 11 pyrene subunits and the other with 17 subunits. In addition, a 11/17 units pGNR heterostructure connected via a pentagon ring junction was modeled. The TB calculated molecular energy levels of the three structures are displayed in Fig. 5. From the energy positions, it is obvious that the molecular energy states of the 11 and 17 units pGNR segments match those of the 11/17 heterostructure and there is no additional energy state despite the fusion between the two pGNR segments. The assignments of the molecular energy states of the 11/17 heterostructure to the two corresponding pGNR segments can be also validated by looking at the wave functions of their molecular states (see Figs. S2–S4 in the ESM).

3 Conclusions

In conclusion, we have investigated longitudinally fused pGNR segments which have different lengths. We find that the pGNR segments are connected by a 5-membered pentagon junction, which however does not induce electronic hybridizations between the fused pGNR segments as reflected by our STS measurements and TB calculations. Therefore, the molecular states of the heterostructure are derived from those of the individual GNR segments and their density of states spatially localized on the respective segments. We expect that the covalent fusion between the pGNR segments may allow for electron transport through those localized states, and is useful for potential applications in single-molecule based electronics and optoelectronics.

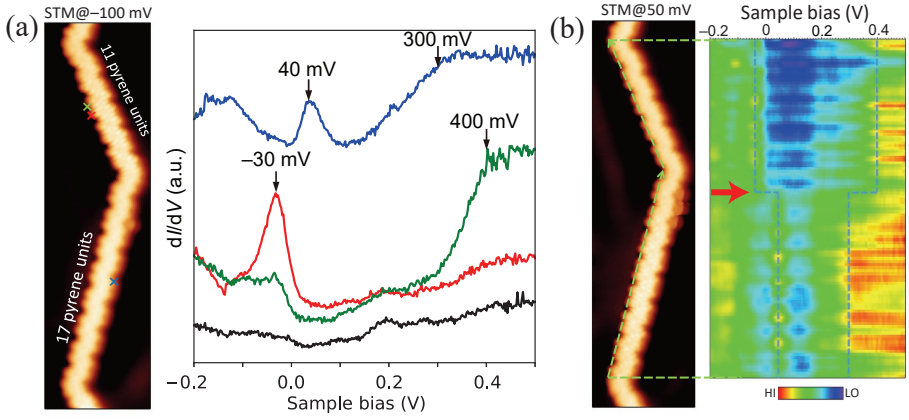

Figure 4 Energy levels of the 11/17 units pGNR heterostructure. (a) STM image of the 11/17 units pGNR heterostructure (V_s = −0.1 V and I_t = 110 pA) and point STS spectra acquired at the positions marked on the STM image with the corresponding colors. The reference spectrum on Au(111) is colored in black. (b) STM image of the 11/17 units pGNR heterostructure (V_s = −0.1 V and I_t = 100 pA) and the color-coded map of the STS spectra acquired along the green line indicated in the STM image. The dark dashed lines indicate HOMO–LUMO level shift across the kink. The gap shift is highlighted by a red arrow.

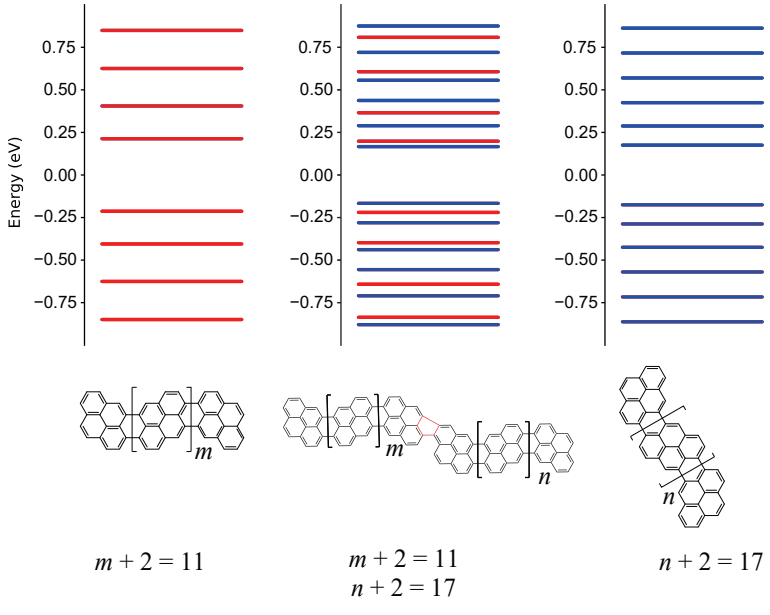

Figure 5 Frontier energy states of the 11 units pGNR segment, 17 units pGNR segment, and the 11/17 units pGNR heterostructure based on TB calculation. The energy states derived from the 11 units pGNR are in red and those from the 17 unit are in blue. Their corresponding chemical structures are shown below, *m* and *n* represent the number of constituting pyrene units minus two.

Acknowledgements

The authors acknowledge the financial support from the National Natural Science Foundation of China (No. 22072086). The Swiss National Science Foundation (Nos. 200020_182015 and 200021_172527) supported this work.

Funding note: Open Access funding provided by Lib4RI – Library for the Research Institutes within the ETH Domain: Eawag, Empa, PSI & WSL.

Electronic Supplementary Material: Supplementary material (reaction path of forming the 5-membered pentagon ring, TB calculated frontier orbitals, methods of STM/STS and nc-AFM characterization and tight-binding calculations) is available in the online version of this article at https://doi.org/10.1007/s12274-022-4410-7.

References

[1] Son, Y. W.; Cohen, M. L.; Louie, S. G. Energy gaps in graphene nanoribbons. *Phys. Rev. Lett.* **2006**, *97*, 216803.

[2] Chen, Y. C.; De Oteyza, D. G.; Pedramrazi, Z.; Chen, C.; Fischer, F. R.; Crommie, M. F. Tuning the band gap of graphene nanoribbons synthesized from molecular precursors. *ACS Nano* **2013**, *7*, 6123–6128.

[3] Ritter, K. A.; Lyding, J. W. The influence of edge structure on the electronic properties of graphene quantum dots and nanoribbons. *Nat. Mater.* **2009**, *8*, 235–242.

[4] Shams, S. S.; Zhang, R. Y.; Zhu, J. Graphene synthesis: A review. *Mater. Sci. Pol.* **2015**, *33*, 566–578.
[5] Narita, A.; Wang, X. Y.; Feng, X. L.; Müllen, K. New advances in nanographene chemistry. *Chem. Soc. Rev.* **2015**, *44*, 6616–6643.
[6] Zhou, X. H.; Yu, G. Modified engineering of graphene nanoribbons prepared via on-surface synthesis. *Adv. Mater.* **2020**, *32*, 1905957.
[7] Lipton-Duffin, J. A.; Ivasenko, O.; Perepichka, D. F.; Rosei, F. Synthesis of polyphenylene molecular wires by surface-confined polymerization. *Small* **2009**, *5*, 592–597.
[8] Cai, J. M.; Ruffieux, P.; Jaafar, R.; Bieri, M.; Braun, T.; Blankenburg, S.; Muoth, M.; Seitsonen, A. P.; Saleh, M.; Feng, X. et al. Atomically precise bottom-up fabrication of graphene nanoribbons. *Nature* **2010**, *466*, 470–473.
[9] Basagni, A.; Sedona, F.; Pignedoli, C. A.; Cattelan, M.; Nicolas, L.; Casarin, M.; Sambi, M. Molecules-oligomers-nanowires-graphene nanoribbons: A bottom-up stepwise on-surface covalent synthesis preserving long-range order. *J. Am. Chem. Soc.* **2015**, *137*, 1802–1808.
[10] Zhang, H. M.; Lin, H. P.; Sun, K. W.; Chen, L.; Zagranyarski, Y.; Aghdassi, N.; Duhm, S.; Li, Q.; Zhong, D. Y.; Li, Y. Y. et al. On-surface synthesis of rylene-type graphene nanoribbons. *J. Am. Chem. Soc.* **2015**, *137*, 4022–4025.
[11] Barin, G. B.; Fairbrother, A.; Rotach, L.; Bayle, M.; Paillet, M.; Liang, L. B.; Meunier, V.; Hauert, R.; Dumslaff, T.; Narita, A. et al. Surface-synthesized graphene nanoribbons for room temperature switching devices: Substrate transfer and *ex situ* characterization. *ACS Appl. Nano Mater.* **2019**, *2*, 2184–2192.
[12] Teeter, J. D.; Costa, P. S.; Pour, M. M.; Miller, D. P.; Zurek, E.; Enders, A.; Sinitskii, A. Epitaxial growth of aligned atomically precise chevron graphene nanoribbons on Cu (111). *Chem. Commun.* **2017**, *53*, 8463–8466.
[13] Ruffieux, P.; Wang, S. Y.; Yang, B.; Sánchez-Sánchez, C.; Liu, J.; Dienel, T.; Talirz, L.; Shinde, P.; Pignedoli, C. A.; Passerone, D. et al. On-surface synthesis of graphene nanoribbons with zigzag edge topology. *Nature* **2016**, *531*, 489–492.
[14] Rizzo, D. J.; Veber, G.; Jiang, J. W.; McCurdy, R.; Cao, T.; Bronner, C.; Chen, T.; Louie, S. G.; Fischer, F. R.; Crommie, M. F. Inducing metallicity in graphene nanoribbons via zero-mode superlattices. *Science* **2020**, *369*, 1597–1603.
[15] Sun, Q.; Gröning, O.; Overbeck, J.; Braun, O.; Perrin, M. L.; Barin, G. B.; El Abbassi, M.; Eimre, K.; Ditler, E.; Daniels, C. et al. Massive Dirac fermion behavior in a low bandgap graphene nanoribbon near a topological phase boundary. *Adv. Mater.* **2020**, *32*, 1906054.
[16] Carbonell-Sanromà, E.; Hieulle, J.; Vilas-Varela, M.; Brandimarte, P.; Iraola, M.; Barragán, A.; Li, J. C.; Abadia, M.; Corso, M.; Sánchez-Portal, D. et al. Doping of graphene nanoribbons via functional group edge modification. *ACS Nano* **2017**, *11*, 7355–7361.
[17] Kawai, S.; Nakatsuka, S.; Hatakeyama, T.; Pawlak, R.; Meier, T.; Tracey, J.; Meyer, E.; Foster, A. S. Multiple heteroatom substitution to graphene nanoribbon. *Sci. Adv.* **2018**, *4*, eaar7181.
[18] Pedramrazi, Z.; Chen, C.; Zhao, F. Z.; Cao, T.; Nguyen, G. D.; Omrani, A. A.; Tsai, H. Z.; Cloke, R. R.; Marangoni, T.; Rizzo, D. J. et al. Concentration dependence of dopant electronic structure in bottom-up graphene nanoribbons. *Nano Lett.* **2018**, *18*, 3550–3556.
[19] Palacios, J. J.; Fernández-Rossier, J.; Brey, L.; Fertig, H. A. Electronic and magnetic structure of graphene nanoribbons. *Semicond. Sci. Technol.* **2010**, *25*, 033003.
[20] Yang, L.; Park, C. H.; Son, Y. W.; Cohen, M. L.; Louie, S. G. Quasiparticle energies and band gaps in graphene nanoribbons. *Phys. Rev. Lett.* **2007**, *99*, 186801.
[21] Wakabayashi, K.; Sasaki, K. I.; Nakanishi, T.; Enoki, T. Electronic states of graphene nanoribbons and analytical solutions. *Sci. Technol. Adv. Mater.* **2010**, *11*, 054504.
[22] Nilius, N.; Wallis, T. M.; Ho, W. Development of one-dimensional band structure in artificial gold chains. *Science* **2002**, *297*, 1853–1856.
[23] Söde, H.; Talirz, L.; Gröning, O.; Pignedoli, C. A.; Berger, R.; Feng, X. L.; Müllen, K.; Fasel, R.; Ruffieux, P. Electronic band dispersion of graphene nanoribbons via Fourier-transformed scanning tunneling spectroscopy. *Phys. Rev. B* **2015**, *91*, 045429.
[24] Gross, L.; Mohn, F.; Moll, N.; Liljeroth, P.; Meyer, G. The chemical structure of a molecule resolved by atomic force microscopy. *Science* **2009**, *325*, 1110–1114.
[25] Kimouche, A.; Ervasti, M. M.; Drost, R.; Halonen, S.; Harju, A.; Joensuu, P. M.; Sainio, J.; Liljeroth, P. Ultra-narrow metallic armchair graphene nanoribbons. *Nat. Commun.* **2015**, *6*, 10177.
[26] Li, J. C.; Sanz, S.; Corso, M.; Choi, D. J.; Peña, D.; Frederiksen, T.; Pascual, J. I. Single spin localization and manipulation in graphene open-shell nanostructures. *Nat. Commun.* **2019**, *10*, 200.
[27] Mishra, S.; Beyer, D.; Berger, R.; Liu, J. Z.; Gröning, O.; Urgel, J. I.; Müllen, K.; Ruffieux, P.; Feng, X. L.; Fasel, R. Topological defect-induced magnetism in a nanographene. *J. Am. Chem. Soc.* **2020**, *142*, 1147–1152.
[28] Zheng, Y. Q.; Li, C.; Zhao, Y.; Beyer, D.; Wang, G. Y.; Xu, C. Y.; Yue, X. L.; Chen, Y. P.; Guan, D. D.; Li, Y. Y. et al. Engineering of magnetic coupling in nanographene. *Phys. Rev. Lett.* **2020**, *124*, 147206.
[29] Lawrence, J.; Brandimarte, P.; Berdonces-Layunta, A.; Mohammed, M. S. G.; Grewal, A.; Leon, C. C.; Sánchez-Portal, D.; De Oteyza, D. G. Probing the magnetism of topological end states in 5-armchair graphene nanoribbons. *ACS Nano* **2020**, *14*, 4499–4508.
[30] Merino-Díez, N.; Garcia-Lekue, A.; Carbonell-Sanromà, E.; Li, J. C.; Corso, M.; Colazzo, L.; Sedona, F.; Sánchez-Portal, D.; Pascual, J. I.; De Oteyza, D. G. Width-dependent band gap in armchair graphene nanoribbons reveals Fermi level pinning on Au (111). *ACS Nano* **2017**, *11*, 11661–11668.